Solid-State Thermal Transformation of Methylammonium Monomolybdate to Polyoxomolybdates and their Applications as Staining Reagents for Transmission Electron Microscopy Observations of Viruses

Ndaru C. Sukmana, [1] Sugiarto, [1] Jun Shinogi, [1] Tatsuhiro Kojima, [2] Akifumi Higashiura, [3] Akima Yamamoto, [3] Takemasa Sakaguchi, [3] and Masahiro Sadakane *[1]

[1]*Department of Applied Chemistry, Graduate School of Engineering, Hiroshima University, 1-4-1 Kagamiyama, Higashi-Hiroshima, 739-8527, Japan*

[2]*Department of Chemistry, Graduate School of Science, Osaka University, 1-1, Machikaneyama, Toyonaka, Osaka, 560-0043, Japan*

[3]*Department of Virology, Graduate School of Biomedical and Health Sciences, Hiroshima University, 1-2-3 Kasumi, Minami-ku, Hiroshima, 734-8551, Japan*

E-mail: sadakane09@hiroshima-u.ac.jp

The solid-state heating of methylammonium monomolybdate, $(CH_3NH_3)_2[MoO_4]$ (prepared by dissolving MoO_3 in an aqueous methylamine solution), in air released methylamine and water to produce $(CH_3NH_3)_6[Mo_7O_{24}]$ and followed by $(CH_3NH_3)_8[Mo_{10}O_{34}]$ before transformation to MoO_3. We report the first single-crystal X-ray structural analysis of $(CH_3NH_3)_2[MoO_4]$ and $(CH_3NH_3)_6[Mo_7O_{24}]$ and demonstrate that the decamolybdate structure is different from that obtained from ammonium molybdates. Furthermore, $(CH_3NH_3)_6[Mo_7O_{24}]$ is a good negative staining reagent for transmission electron microscopy observations of viruses, such as SARS-CoV-2 and influenza virus.

Keywords: Polyoxometalate, Thermal transformation, Negative staining reagent.

Polyoxometalates (POMs) are anionic polynuclear metal–oxo molecules of early transition metals, such as W, Mo, V, and Nb, formed between metal oxides (WO_3 or MoO_3) and monometalates ($[WO_4]^{2-}$ or $[MoO_4]^{2-}$). These molecule have been extensively investigated because their structures and composites can be modified through various techniques to tune their unique acidic, redox, magnetic, chemical, and physical properties.[1–3]

In particular, isopolyoxomolybdates containing Mo as the sole metal component have been utilized as corrosion inhibitors,[4,5] supercapacitors,[6] anticancer agents,[7] and starting Mo sources for Mo-based oxide materials.[8,9] Notably, monomolybdate, $[MoO_4]^{2-}$, prepared by dissolving MoO_3 in a base, such as NaOH and KOH, presents in a basic to neutral solution. The addition of an acids condenses monomolybdate to polyoxomolybdates, such as $[Mo_7O_{24}]^{6-}$, $[Mo_8O_{26}]^{4-}$, and $[Mo_{36}O_{112}(H_2O)_{16}]^{8-}$ with dehydration in aqueous solutions (Scheme S1).[3,10,11] The dehydrative condensation degrees and, often, the sizes of the molecules increase with the addition of more acids until they are completely converted to MoO_3.

It is known that solid-state heating of the ammonium salt of molybdates produces an effect similar to acid addition. Dissolving MoO_3 in an ammonia solution produces $(NH_4)_2[MoO_4]$. The volatile NH_3 and water produced by NH_4^+ and the oxygen atoms of metalates are eliminated by heating, and condensation is promoted in the solid state. Further, the solid-state heating of $(NH_4)_2[MoO_4]$ is known to produce several ammonium isomolybdates, such as $(NH_4)_2[Mo_2O_7]$, $(NH_4)_2[Mo_3O_{10}]$, and $(NH_4)_2[Mo_4O_{13}]$ (same as $(NH_4)_4[Mo_8O_{26}]$),[12] and further heating produces hexagonal-MoO_3 and orthorhombic-MoO_3 (Scheme S2).[13]

In addition, dissolving MoO_3 in an ethylenediamine solution produces ethylenediammonium monomolybdate, $(NH_3CH_2CH_2NH_3)[MoO_4]$, which is continuously converted to $(NH_3CH_2CH_2NH_3)_2[Mo_2O_7]$, $(NH_2CH_2CH_2NH_2)MoO_3$, and MoO_3 via solid-state heating.[14]

We aimed investigate polyoxometates produced by reactions between metal oxides and a volatile base methylamine (CH_3NH_2); accordingly, we recently reported that the reaction of WO_3 or V_2O_5 with methylamine and subsequent drying produced methylammonium paradodecatungstate, $(CH_3NH_3)_{10}[H_2W_{12}O_{42}]$,[15] or methylammonium vanadate, $CH_3NH_3[VO_3]$,[16] respectively. One of our authors indicated that dissolving MoO_3 in an aqueous methylamine solution and subsequent drying (under vacuum at 70 °C) produced methylammonium heptamolybdate, $(CH_3NH_3)_6[Mo_7O_{24}]$, which was a suitable Mo source for the production of orthorhombic Mo–V based mixed oxides,[17,18] which is among the most promising oxidation catalysts.[19] Notably, $(CH_3NH_3)_6[Mo_7O_{24}]$ was characterized via Raman spectroscopy and elemental analysis; however, an analysis of the molecular structure via single-crystal X-ray structural analysis is yet to be conducted. Therefore, it is crucial to understand the true structure and heating effect on the methylammonium molybdate.

Methylammonium monomolybdate, $(CH_3NH_3)_2[MoO_4]$, was prepared by dissolving MoO_3 in a 40% methylamine solution at a methylamine/Mo ratio of 4, followed by subsequent precipitation with the addition of N,N-dimethylformamide (DMF) (Schemes 1 and S3).

Single-crystal X-ray structural analysis revealed that monomolybdate, $[MoO_4]^{2-}$, crystallized in the space group *Pnma*, together with two methylammonium ($CH_3NH_3^+$) counter cations (Figures 1(a), 1(b), and Table S1). Four oxygen atoms surrounded the molybdenum cation tetrahedrally (Figure 1(a) and S1) with O–Mo–O angles between 108.98° and 109.95° (Table S2). The Mo–O distances were found to be nearly equal between 1.75 and 1.78 Å (Table S3), which are comparable to the average tetrahedral Mo–O distances found in K_2MoO_4 (1.76 Å)[20] and $(NH_4)_2MoO_4$ (1.76 Å).[21] Typically, the $[MoO_4]^{2-}$ ion forms hydrogen bonds with methylammonium via N–H···O interactions (Figure S1) with distances of 2.73 to 2.82 Å.

In our analysis, the powder X-ray diffraction (XRD) pattern simulated using single-crystal structure data fitted well with the experimental XRD patterns (Figures 2(a) and

S2), indicating that the obtained solid exhibits the same crystal structure, and the phase purity of the bulk powders was satisfactory. The difference in peak intensities between the simulation and experimental results could be attributed to the preferred orientation of the powder sample.

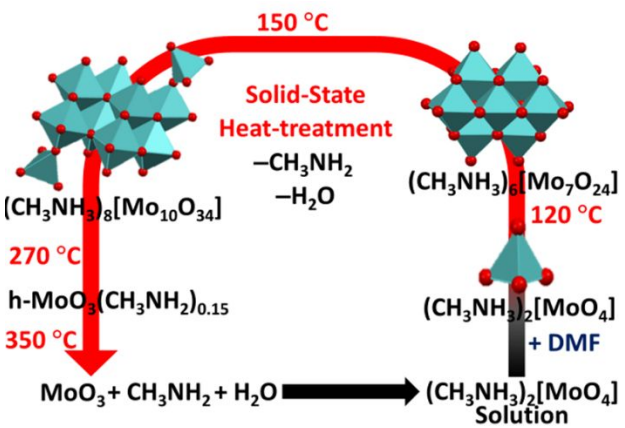

Scheme 1. Formation of methylammonium isopolyoxomolybdates by the reaction of MoO_3 with a CH_3NH_2 solution and subsequent heating.

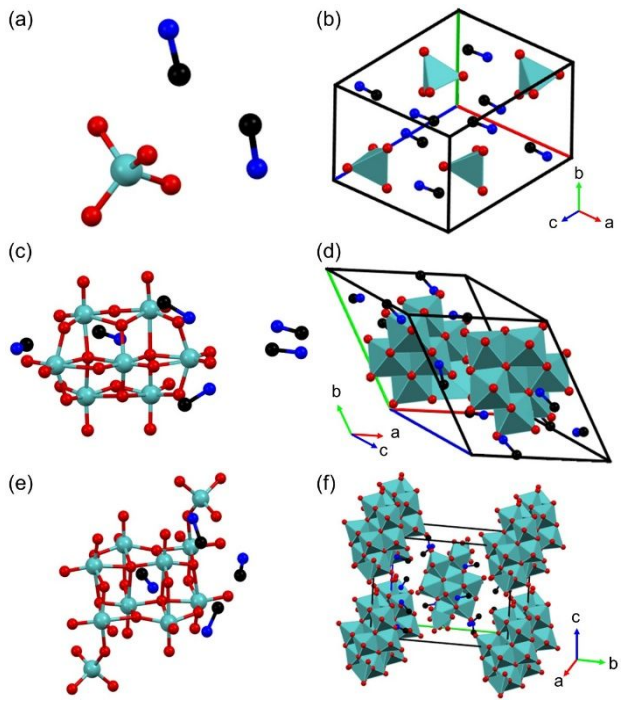

Figure 1. Ball-and-stick representation of methylammonium molybdates and packing of the molecules in a unit cell. (a and b) methylammonium monomolybdate, $(CH_3NH_3)_2[MoO_4]$, (c and d) methylammonium heptamolybdate, $(CH_3NH_3)_6[Mo_7O_{24}]$, and (e and f) methylammonium decamolybdate, $(CH_3NH_3)_8[Mo_{10}O_{34}]$. Light blue, red, black, and blue balls represent Mo, O, C, and N atoms, respectively.

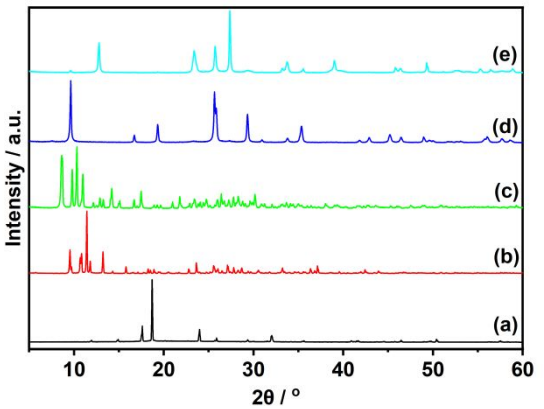

Figure 2. XRD patterns of (a) methylammonium monomolybdate calcined at (b) 120, (c) 150, (d) 270, and (e) 350 °C.

The Fourier transform infrared (FT-IR) spectrum (Figures S3 and S4(a)) presents bands at 1467 and 1261 cm^{-1}, which can be attributed to NH_3^+ bending and CH_3–NH_3^+ rocking, respectively. Furthermore, the IR band at 956 cm^{-1} can be assigned to the symmetric stretching vibration of $[MoO_4]^{2-}$, and the bands at 833, 879, and 898 cm^{-1} may be assigned to the asymmetric stretching vibration of $[MoO_4]^{2-}$.[22]

The Raman band around 1001 cm^{-1} can be assigned to the C–N stretching vibration, which indicates the presence of methylammonium as a counter cation (Figures S5 and S6(a)). The strong Raman bands at 898 and 315 cm^{-1} can be attributed to the symmetric stretching and bending of $[MoO_4]^{2-}$, respectively. In addition, the Raman band at 838 cm^{-1} can be assigned to the asymmetric stretching of MoO_4 units.[23]

The solution Raman spectrum was found to be similar to the solid-state spectrum (Figures S5(c) and S5(d)), and the ultraviolet-visible (UV–vis) spectrum presented a peak at 207 nm and a shoulder near 230 nm (Figure S7), in agreement with the spectrum of $[MoO_4]^{2-}$ reported in the literature.[24] These results indicate the presence of $[MoO_4]^{2-}$ in the reaction mixture.

The thermogravimetry–differential thermal analysis (TG–DTA) diagram of methylammonium monomolybdate in air flow indicates approximately 36% weight loss up to 450 °C, which indicates the consumption of 2 mol of methylamine and 1 mol water from $(CH_3NH_3)_2[MoO_4]$ to form MoO_3 (36%) (Figure S8 and Table S4). For $(NH_4)_2[MoO_4]$,[13] and $(NH_3CH_2CH_2NH_3)[MoO_4]$,[14] the TG curves present stepwise weight losses, clearly indicating a transformation of the molybdate structure. However, several gradual weight losses can be observed; the first one between 80 and 150 °C with an endothermic peak, the second one between 150 and 350 °C with small exothermic peaks, and the third at approximately 400 °C with a large exothermic peak.

We discovered that the powder XRD patterns were altered after solid-state heating in air (Figure 2, Schemes 1 and S3). The first transformation was observed by heating methylammonium monomolybdate at 120 °C for 1 h (Figure

2(b)). The observed powder XRD pattern was found to be similar to one that reported in our previous paper.[18] We discovered that a single-crystal could be obtained with the addition of DMF to an aqueous solution of the heated solid. Further, single-crystal X-ray structure analysis revealed that the crystal contained heptamolybdate, an $[Mo_7O_{24}]^{6-}$ anion, and six methylammonium cations (Figures 1(c), 1(d), and Table S1). Note that the $[Mo_7O_{24}]^{6-}$ anion comprises seven condensed edge-sharing MoO_6 octahedra (Figures 1(c), 1(d) and S9)), similar to the reported heptamolybdate anion for ammonium and sodium salts.[25,26] The Mo–O distances were found to be 1.71 to 2.64 Å, and the bond angles O–Mo–O were found to be 70.11 to 174.81° (Tables S5 and S6). The crystal structure revealed the presence of hydrogen bonding interactions between the $CH_3NH_3^+$ cations and the $[Mo_7O_{24}]^{6-}$ anions (Figure S9). The peak positions in the experimental powder XRD profiles matched with those in the simulated powder XRD pattern obtained from single-crystal X-ray data (Figure S10), implying that the powder had high phase purity. Furthermore, the formula was also confirmed via TG–DTA and CHN elemental analysis (Table S4). These results indicate that the true structure of $[Mo_7O_{24}]^{6-}$ reported in our previous paper[18] corresponds to that of the common heptamolybdate.

The IR bands at 921, 892, and 840 cm^{-1} represent the stretching vibrations of Mo=O from the heptamolybdate anion (Figure S4(b)). The strong Raman bands at 936 and 885 cm^{-1} can be attributed to the asymmetric stretching vibration of the Mo=O bond in $[Mo_7O_{24}]^{6-}$ (Figure S6(b)).

The second powder XRD transformation was observed by heating at 150 °C for 1 h (Figure 2(c)). Further, single crystals of the heated solid were obtained via recrystallization. The single-crystals X-ray structure analysis revealed that the obtained solid was methylammonium decamolybdate, $(CH_3NH_3)_8[Mo_{10}O_{34}]\cdot 2H_2O$, which is known to crystallize in the space group monoclinic, $P2_1/n$ (Figures 1(e), 1(f), and Table S1). Notably, the anion comprises $[\gamma\text{-}Mo_8O_{26}]$,[27] which is composed of eight MoO_6 octahedra connected via edge-sharing and two MoO_4 tetrahedra connected to the $[\gamma\text{-}Mo_8O_{26}]$ unit by corner-sharing (Figures 1(e), 1(f), and S11). This structure was the same as that of $(CH_3NH_3)_8[Mo_{10}O_{34}]\cdot 2H_2O$ prepared by a reaction of $(NH_4)_6[Mo_7O_{24}]$ with methylamine, as reported by Yamase et al.[28] The XRD pattern was closely resembled the simulated XRD pattern obtained from single-crystal structural data, indicating the pure nature of the isolated solid (Figure S12).

It is known that the solid-state heating of $(NH_4)_6[Mo_7O_{24}]$ at approximately 100–200 °C produces ammonium decamolybdate, $(NH_4)_8[Mo_{10}O_{34}]$ (Scheme S4).[13,29] However, connections between the MoO_4 tetrahedra and the $[\gamma\text{-}Mo_8O_{26}]$ unit of methylammonium decamolybdate are different from those in ammonium decamolybdate produced by heating ammonium heptamolybdate. In methylammonium decamolybdate, MoO_4 units are connected to the linking sites O14, whereas in ammonium decamolybdate, they are located at the site O13 (Figure S13).

The Mo–O distances were found to be between 1.7 and 2.43 Å, and the bond angles O–Mo–O were identified to be between 69.07 and 164.21° (Tables S7 and S8). The crystal structure revealed the presence of hydrogen bonding interactions between the $CH_3NH_3^+$ cations and $[Mo_{10}O_{34}]^{8-}$ anions (Figure S11). The TG–DTA and CHN analysis also confirmed the formula of the solid (Table S4).

The Raman band observed at 1005 cm^{-1} can be assigned to C–N stretching in methylammonium as a counter cation (Figure S6(c)). The characteristic Raman bands of the decamolybdate anion were observed at 953, 934, 919, 899, 876, 854, and 675 cm^{-1}, and the strong band at 953 cm^{-1} could be attributed to the stretching vibrations of the Mo=O bond in decamolybdate.[30] The formation of the decamolybdate anion and the presence of methylammonium cation were also confirmed via the FT-IR analysis (Figure S4(c)).

Further heating at 270 and 350 °C for 1 h produced hexagonal-MoO_3 (Figures 2(d) and S14) and orthorhombic-MoO_3 (Figures 2(e) and S15), respectively.

Our results clearly indicate that the polyoxomolybdate species obtained by the solid-state thermal transformation of $(CH_3NH_3)_2[MoO_4]$ are different from those obtained using $(NH_4)_2[MoO_4]$ (Schemes 1, S2, and S3). Previous studies have reported that the types of the counter cations affect the formation of polyoxometalates in solutions.[10,11,29] Notably, the heating of methylammonium polyoxomolybdates releases methylamine and water molecules, which alters their structure. Additionally, basicity differences (the pKb of CH_3NH_2 and NH_3 is 3.34 and 4.75, respectively) and the boiling temperature of the base (−6.3 and −33.3 °C for CH_3NH_2 and NH_3, respectively) may also affect the formation temperature and the formed polyoxometalates.

Previously, Szilágyi et al. reported that $(NH_4)_2[MoO_4]$ was transformed to a mixture of $(NH_4)_2[Mo_3O_{10}]$ and $(NH_4)_2[Mo_2O_7]$ after heating at 205 °C, $(NH_4)_2[Mo_4O_{13}]$ after heating at 230 °C, and orthorhombic MoO_3 after heating at 370 °C in air (Scheme S2).[13] Further, Ressler et al. reported that the structure of $(NH_4)_2[Mo_4O_{13}]$ was equivalent to the structure of $(NH_4)_4[Mo_8O_{26}]$ in that γ-type octamolybdates were connected to each other via edge-sharing.[12]

By contrast, we discovered that $(CH_3NH_3)_2[MoO_4]$ was transformed to $(CH_3NH_3)_6[Mo_7O_{24}]$ at 120 °C, $(CH_3NH_3)_8[Mo_{10}O_{34}]$ at 150 °C, hexagonal-$MoO_3(CH_3NH_2)_{0.15}$ at 270 °C, and orthorhombic-MoO_3 at 350 °C (Schemes 1 and S3).

Further investigations on the solid-state thermal heating of methylammonium polyoxomolybdates are now underway.

Notably, for virology, observing of the viral shape are particularly important, and transmission electron microscopy (TEM) with heavy metal negative staining reagents is the most widely used technique.[31] We were motivated by the desire to develop new negative staining reagents using polyoxometalates.[16,32,33] Methylammonium vanadate and tungstate have been commercialized to observe viruses via TEM, and this is indicative of the importance of methylammonium cations.[34,35] However, methylammonium molybdates are yet to be applied for this purpose.

The produced molybdates were dissolved in water (0.5 wt%), and the solution was contacted with viruses attached to a carbon support film for TEM; note that the excess solution was removed and dried before TEM observations.[32] Notably, methylammonium decamolybdate, $(CH_3NH_3)_8[Mo_{10}O_{34}]$,

could not be dissolved at 0.5 wt% in water at room temperature. Methylammonium heptamolybdate was found to be a good staining reagent for observing the SARS-CoV-2 delta variant, as evaluated by the contrast and sharpness of the stained particles (Figures 3(a)-(c)). Virus particles with diameters of approximately 85–120 nm and spike lengths of 15–35 nm were observed,[36] which were in agreement with those previously reported.[37] The spikes could not clearly be observed by using the $(CH_3NH_3)_2[MoO_4]$ (Figure 3(d)). This result indicates that the selection of molybdate structure is an essential factor for clear observation. Furthermore, the SARS-CoV-2 omicron variant (Figure 3(e)) and influenza virus (Figure 3(f)) could be clearly observed using the methylammonium heptamolybdate.

Further effort aimed at understanding the interactions between polyoxomolybdates and virions and the develop of better negative staining reagents are underway.

In conclusion, we clearly observed the solid-state thermal conversion of monomolybdate, $[MoO_4]^{2-}$, to MoO_3 through the following two polyoxomolybdates: $[Mo_7O_{24}]^{6-}$ and $[Mo_{10}O_{34}]^{8-}$ with the methylammonium cation (Schemes 1 and S3), and the results obtained via single-crystal structural analyses of $(CH_3NH_3)_2[MoO_4]$ and $(CH_3NH_3)_6[Mo_7O_{24}]$ are presented herein for the first time. Particularly, the observed thermal transformation was found to be different from that observed using ammonium monomolybdate. Furthermore, we identified $(CH_3NH_3)_6[Mo_7O_{24}]$ to be a suitable negative staining reagent for observation of SARS-CoV-2 and influenza virus using TEM observations. However, further investigation on thermal transformations and virus observations are underway.

This research was supported by a JSPS KAKENHI Grant-in-Aid for Scientific Research (A) (JP19H00843), Grant-in-Aid for Transformative Research Area (A) "Supra-ceramics (JP22H05144), JST A-STEP (Grant Number JPMJTM20RF), Research Grant for COVID-19 from AMED under Grant Number JP21fk0108550, Mitsubishi Chemical Co., International Network on Polyoxometalate Science at Hiroshima University, and JSPS Core-to-Core program. N. C. S. would like to thank the financial support from the Osimo Scholarship and Program for Developing and Supporting the Next Generation of Innovative Researchers at Hiroshima University. The authors are grateful to Ms. M. Kosaka and Mr. M. Kobayashi at Division of Instrumental Analysis, Okayama University for their help in CHN elemental analyses and Ms. K. Koike at the Natural Science Center for Basic Research and Development, Hiroshima University for support in TEM analysis. Synchrotron radiation experiments were performed on BL02B1 at Spring-8 with the approval of the Japan Synchrotron Radiation Research Institute (JASRI) (Proposal No. 2020 A1795).

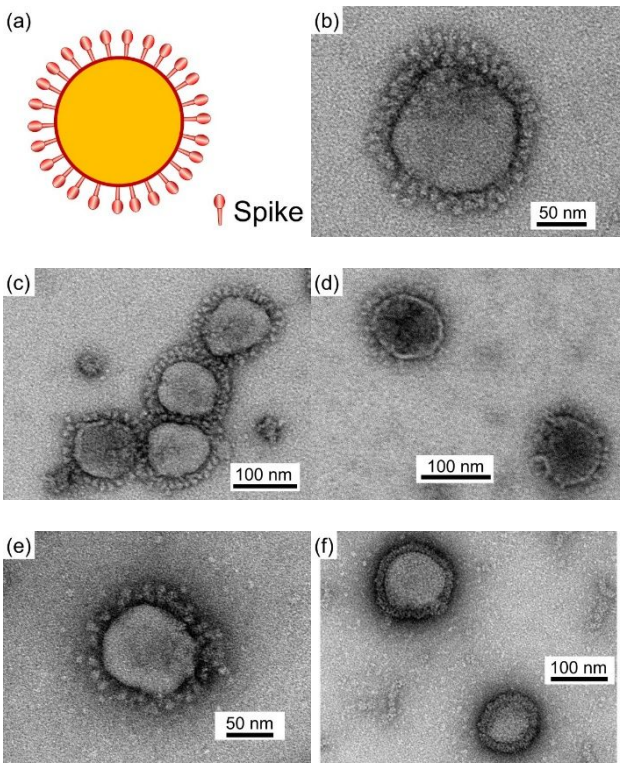

Figure 3. (a) Schematic 2D-morphology of corona virion. TEM images of SARS-CoV-2 delta variant virions stained using (b and c) methylammonium heptamolybdate and (d) methylammonium monomolybdate. TEM images of (e) SARS-CoV-2 omicron variant virions and (f) influenza virions stained using methylammonium heptamolybdate.

Supporting Information is available on http://dx.doi.org/10.1246/cl.******.

References and Notes

1. L. Cronin (Ed.), *Chem. Soc. Rev.* **2012**, *41*, 7325–7648.
2. C. L. Hill (Ed.), *Chem. Rev.* **1998**, *98*, 1–390.
3. M. T. Pope, *Heteropoly and Isopoly Oxometalates*, Springer-Verlag, Berlin, **1983**.
4. D. S. Kharitonov, M. Zimowska, J. Ryl, A. Zieliński, M. A. Osipenko, J. Adamiec, A. Wrzesińska, P. M. Claesson, I. I. Kurilo, *Corros. Sci.* **2021**, *190*, 109664.
5. I. A. W. Ma, S. Ammar, S. S. A. Kumar, K. Ramesh, S. Ramesh, *J. Coat. Technol. Res* **2022**, *19*, 241–268.
6. L. Zhang, S. Zheng, L. Wang, H. Tang, H. Xue, G. Wang, *Small* **2017**, *13*, 1700917.
7. H. Yanagie, A. Ogata, S. Mitsui, T. Hisa, T. Yamase, M. Eriguchi, *Biomed. Pharmacother.* **2006**, *60*, 349–352.
8. I. A. De Castro, R. S. Datta, J. Z. Ou, A. Castellanos-gomez, S. Sriram, T. Daeneke, K. Kalantar-zadeh, *Adv. Mater.* **2017**, *29*, 1701619.
9. K. H. Kang, G. T. Kim, S. Park, P. W. Seo, H. Seo, C. W. Lee, *J. Ind. Eng. Chem.* **2019**, *76*, 1–16.
10. N. I. Gumerova, A. Rompel, *Chem. Soc. Rev.* **2020**, *49*, 7568–7601.

11. S. Himeno, H. Niiya, T. Ueda, *Bull. Chem. Soc. Jpn.* **1997**, *70*, 631–637.
12. J. Wienold, R. E. Jentoft, T. Ressler, *Eur. J. Inorg. Chem.* **2003**, 1058–1071.
13. T. N. Kovács, D. Hunyadi, A. L. A. de Lucena, I. M. Szilágyi, *J. Therm. Anal. Calorim.* **2016**, *124*, 1013–1021.
14. W. Bensch, P. Hug, R. Emmenegger, A. Reller, H. R. Oswald, *Mat. Res. Bull.* **1987**, *22*, 447–454.
15. N. C. Sukmana, Sugiarto, Z. Zhang, M. Sadakane, *Z. Anorg. Allg. Chem.* **2021**, *647*, 1930–1937.
16. N. C. Sukmana, J. Shinogi, A. Yamamoto, A. Higashiura, T. Sakaguchi, M. Sadakane, *Eur. J. Inorg. Chem.* **2022**, e202200322.
17. S. Ishikawa, Y. Yamada, C. Qiu, Y. Kawahara, N. Hiyoshi, A. Yoshida, W. Ueda, *Chem. Mater.* **2019**, *31*, 1408–1417.
18. S. Ishikawa, T. Murayama, S. Ohmura, M. Sadakane, W. Ueda, *Chem. Mater.* **2013**, *25*, 2211–2219.
19. S. Ishikawa, W. Ueda, *Catal. Sci. Technol.* **2016**, *6*, 617–629.
20. B. M. Gatehouse, P. Laverett, *J. Chem. Soc. A* **1969**, 849–854.
21. M. Dittmann, E. Schweda, *Z. Anorg. Allg. Chem.* **1998**, *624*, 2033–2037.
22. S. Vilminot, G. André, M. Richard-Plouet, F. Bourée-Vigneron, M. Kurmoo, *Inorg. Chem.* **2006**, *45*, 10938–10946.
23. V. P. M. Pillai, T. Pradeep, M. J. Bushiri, R. S. Jayasree, V. U. Nayar, *Spectrochim. Acta A Mol. Biomol. Spectrosc.* **1997**, *53*, 867–876.
24. T. Ozeki, H. Kihara, S. Ikeda, *Anal. Chem.* **1988**, *60*, 2055–2059.
25. K. Sjoböm, B. Hedman, *Acta Chem. Scand.* **1973**, *27*, 3673–3691.
26. E. Shimao, *Bull. Chem. Soc. Jpn.* **1967**, *40*, 1609–1613.
27. W. G. Klemperer, W. Shum, *J. Am. Chem. Soc.* **1976**, *98*, 8291–8293.
28. P. K. Bharadwaj, Y. Ohashi, Y. Sasada, Y. Sasaki, T. Yamase, *Acta Crystallogr., Sect. C Struct. Chem.* **1986**, *42*, 545–547.
29. V. W. Day, M. F. Fredrich, W. G. Klemperer, W. Shum, *J. Am. Chem. Soc.* **1977**, *99*, 6146–6148.
30. Y. T. Kim, E. D. Park, *Appl.Catal. A Gen.* **2009**, *361*, 26–31.
31. C. A. Scarff, M. J. G. Fuller, R. F. Thompson, M. G. Iadaza, *J. Vis. Exp.* **2018**, *2018*, 1–8.
32. K. Sahiro, Y. Kawato, K. Koike, T. Sano, T. Nakai, M. Sadakane, *Sci. Rep.* **2022**, *12*, 7554.
33. Y. Kawato, T. Mekata, T. Nishioka, I. Kiryu, T. Sakai, M. Tomoki, S. Miwa, K. Koike, M. Sadakane, K. Mori, *Virology* **2021**, *559*, 120–130.
34. D. M. Shayakhmetov, T. Papayannopoulou, G. Stamatoyannopoulos, A. Lieber, *J. Virol.* **2000**, *74*, 2567–2583.
35. B. Franzetti, G. Schoehn, J.-F. Hernandez, M. Jaquinod, R. W. H. Ruigrok, G. Zaccai, *EMBO J.* **2002**, *21*, 2132–2138.
36. *Virus Taxonomy*, Ninthe Report of the International Committee on Taxonomy of Viruses, ed. by A. M. Q. King, M. J. Adams, E. B. Carstens, E. J. Lefkowitz, Elsevier Academic Press, London, **2012**.
37. H. Yao, Y. Song, Y. Chen, N. Wu, J. Xu, C. Sun, J. Zhang, T. Weng, Z. Zhang, Z. Wu, L. Cheng, D. Shi, X. Lu, J. Lei, M. Crispin, Y. Shi, L. Li, S. Li, *Cell* **2020**, *183*, 730–738.

NOTE *The diagram is acceptable in a colored form. Publication of the colored G.A. is free of charge.*
For publication, electronic data of the colored G.A. should be submitted. Preferred data format is EPS, PS, CDX, PPT, and TIFF.
If the data of your G.A. is "bit-mapped image" data (not "vector data"), note that its print-resolution should be 300 dpi.

You are requested to put a brief abstract (50-60words, one paragraph style) with the graphical abstract you provided, so that readers can easily understand what the graphic shows.

Graphical Abstract

Textual Information

A brief abstract (required)	The release of methylammonium and water while heating methylammonium monomolybdate results in the formation of two methylammonium polyoxomolybdates $(CH_3NH_3)_6[Mo_7O_{24}]$ and $(CH_3NH_3)_8[Mo_{10}O_{34}]$ before transformation to molybdenum oxides such as hexagonal MoO_3 and orthorhombic MoO_3. Methylammonium heptamolybdates can be used as a negative staining reagents for transmission electron microscopy observation of SARS-CoV-2 and influenza viruses.
Title(required)	Solid-State Thermal Transformation of Methylammonium Monomolybdate to Isopolymolybdates and their Applications as Staining Reagents for Transmission Electron Microscopy Observations of Viruses
Authors' Names(required)	Ndaru C. Sukmana, Sugiarto, Jun Shinogi, Tatsuhiro Kojima, Akifumi Higashiura, Akima Yamamoto, Takemasa Sakaguchi, Masahiro Sadakane

Graphical Information

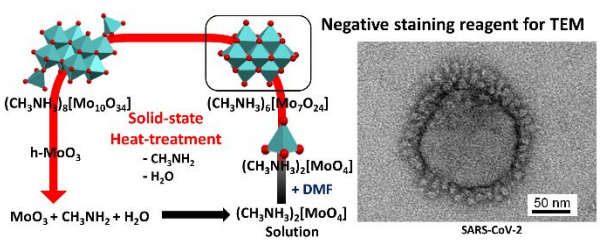

<Please insert your Graphical Abstract:
The size is limited within 100 mm width and 30 mm height, or 48 mm square>(required)

Electronic Supporting Information for *Chemistry Letters*

Supporting information for

Solid-State Thermal Transformation of Methylammonium Monomolybdate to Methylammonium Polyoxomolybbdates and their Applications as Staining Reagents for Transmission Electron Microscopy Observations of Viruses

Ndaru C. Sukmana, Sugiarto, Jun Shinogi, Tatsuhiro Kojima, Akifumi Higashiura, Akima Yamamoto, Takemasa Sakaguchi, Masahiro Sadakane

Experimental Details

Materials. All chemicals were reagent grade. 40% methylamine was purchased from Kanto Chemical CO., Inc., molybdenum trioxide and N,N-dimethylformamide (DMF) were purchased from Wako Pure Chemical Industries, Ltd., and homemade deionized water (Millipore, Elix, USA, MA) was used throughout this study.

Preparation of $(CH_3NH_3)_2[MoO_4]$. MoO_3 (2.1 g, Mo: 15 mmol) was stirred with in a 5 mL 40% methylamine solution in a glass beaker for 30 min at room temperature to a produce clear colorless solution. An excess of DMF (15 mL) was added to the solution, and the resulting white solid (2.28 g) was filtered. Infrared (IR), $\tilde{\nu}$/cm^{-1}(KBr): 3070(s), 2863(m), 2730(m), 2159(m), 1627(m), 1540(m), 1473(m), 1409(w), 1261(w), 958(m, sh), 898(vs), 879(vs), 836(vs), 676921(s, sh), 892(vs), 840 (s), 784(s, sh), 676(s) cm^{-1}. Elemental analysis calcd. for $(CH_3NH_3)_2[MoO_4]$: C 9.92, H 5.84, N 11.57; found, C 10.09, H 5.36, N 11.6.

Preparation of single-crystals of $(CH_3NH_3)_2[MoO_4]$. MoO_3 (0.7 g, Mo: 5 mmol) was stirred in a 40% methylamine solution (1.7 ml) in a glass container for 30 min at room temperature, which produced a clear colorless solution. DMF (1.7 mL) was added to the solution, and colorless crystals were obtained immediately.

Calcination of $(CH_3NH_3)_2[MoO_4]$. $(CH_3NH_3)_2[MoO_4]$ (1 g) was calcined in air to 120, 150, 270, and 450 °C; the temperature was raised at a heating rate of 10 °C/min, and the final temperature was maintained for 1 h in air. $(CH_3NH_3)_6[Mo_7O_{24}]$, $(CH_3NH_3)_8[Mo_{10}O_{34}]\cdot 2H_2O$, hexagonal MoO_3, and orthorhombic MoO_3 were formed at the foregoing temperatures.

$(CH_3NH_3)_6[Mo_7O_{24}]$, $\tilde{\nu}$/cm^{-1}(KBr): 3438(m), 1629(m), 1496(m), 1471(m), 1423(w), 1263(w), 921(s, sh), 892(vs), 840 (s), 676(vs) cm^{-1}. Elemental analysis calcd. for $(CH_3NH_3)_6[Mo_7O_{24}]$: C 5.77, H 2.91, N 6.74; found, C 5.45, H 2.77, N 6.11.

Preparation of single-crystals of $(CH_3NH_3)_6[Mo_7O_{24}]$. 0.1 g of $(CH_3NH_3)_6[Mo_7O_{24}]$ was dissolved in 0.2 mL water, and following this, 0.2 mL of DMF was added to the solution, and this was placed in a closed 10 mL glass vessel. After one day, colorless crystals suitable for single-crystal X-ray structural analysis were obtained.

$(CH_3NH_3)_8[Mo_{10}O_{34}]\cdot 2H_2O$, $\tilde{\nu}$/cm^{-1}(KBr): 3455(m), 1602(m), 1483(m), 1425(w), 1263(w), 912 (s), 873(vs), 840(s), 684(vs) cm^{-1}. Elemental analysis calcd. for $(CH_3NH_3)_8[Mo_{10}O_{34}]\cdot 2H_2O$: C 5.35, H 2.92, N 6.24; found, C 5.15, H 2.62, N 5.85.

Preparation of single-crystals of $(CH_3NH_3)_8[Mo_{10}O_{34}]\cdot 2H_2O$. 0.2 g of the heated solid at 120 °C was dissolved in 0.3 mL water, and this was heated at 60 °C until all solids were completely dissolved. The temperature was gradually decreased to room temperature, and colorless crystals suitable for single-crystal X-ray structural analysis were obtained.

Analytical Techniques. Powder X-ray diffraction (XRD) patterns were obtained using Bruker D2 PHASER 2nd Gen with Cu-Kα radiation. The samples were ground and placed on a sample holder, and the XRD profiles were recorded at 2θ = 3–80°. The Fourier transform infrared (FT-IR) spectra were obtained using a NICOLET 6700 FT-IR spectrometer (Thermo Fischer Scientific) in the range of 650–4000 cm^{-1} with KBr pellets. Thermogravimetry-differential thermal analysis (TG-DTA) was conducted using a TG-DTA7300 instrument (SII, Japan) with an air flow of 200 mL s^{-1}, the heating rate was 10 °C min^{-1}. The temperature was raised at a rate of 10 C° min^{-1} to the target temperature. Ultraviolet–visible (UV–Vis) spectra were obtained using an Agilent 8453 UV–vis spectrometer in the range of 190–1100 nm with a cell length of 1 cm, and the Raman spectra were collected using a JASCO RMP-510 with a 532.0 nm laser; note that each spectrum was recorded for 1 s, and this was repeated three times. CHN analyses were performed at the Division of Instrumental Analysis, Okayama University.

X-ray Crystallography. The single-crystal X-ray diffraction data of $(CH_3NH_3)_2[MoO_4]$, $(CH_3NH_3)_6[Mo_7O_{24}]$, and $(CH_3NH_3)_8[Mo_{10}O_{34}]\cdot 2H_2O$ were collected using Bruker APEX-II CCD at 100 K using monochromatic Mo-Kα radiation (λ=0.71073 Å). Data reduction and space group determination were performed using the Bruker APEX 3 suite.[1] Absorption correction was applied using a multi-scan technique (SADABS).[1] The structure was solved using direct methods with SHELXT[2], and refined using SHELXL[3] with the SHELXle[4] interface. The carbon and nitrogen atoms in the methylammonium cations were located in the electron density map, where the cations were found to be hydrogen bonded to the anionic cluster. The crystal data of methylammonium isopolymolybdate are summarized in Table S1. CCDC 2222172, 2222173, and 2222175 contain crystallographic data for methylammonium monomolybdate, methylammonium heptamolybdate, and methylammonium decamolybdate, respectively, which can be obtained free of charge from the Cambridge Crystallographic Data Centre (CCDC).

Preparation of SARS-CoV-2. SARS-CoV-2/JP/HiroC77/2021 (Delta B.1.617.2, EPI_ISL_6316561) and hCoV-19/Japan/PG-178634/2022 (Omicron BA.1, EPI_ISL_9217693) were prepared via a method described in our previous paper.[5] Virus culturing was performed at the P3 facility of Hiroshima University under Biosafety Level 3 regulations.

Preparation of influenza virus: The human influenza virus [A/Udorn/72 (H3N2)] was propagated in embryonated chicken eggs as described previously.[6] The virus was sedimented via ultracentrifugation at 22000

rpm for 1 h through a 20%(w/w) sucrose/saline layer using a Beckman SW32Ti rotor. The virus pellet was suspended in saline and used for electron microscopy.

TEM observations: For transmission electron microscopy (TEM) analysis, the virus solution (3 μL) was adsorbed onto a glow-discharged (PIB-10, VACUUM DEVICE PIB-10, Ibaraki, Japan) formvar and carbon-coated Cu grid (EM Japan, Tokyo, Japan) for 30 s. The excess solution was eliminated using filter paper. Subsequently, a drop (3 μL) of 0.9%(w/v) NaCl was placed in contact with the grid for 30 s for washing, and then, it was blotted with filter paper. Finally, the staining solution (0.5 wt.% in water) was placed on the grid for 30 s, and the excess solution was removed using filter paper. The staining step was performed twice, and the grid was air dried and irradiated with UV light (Care222™, Ushio Inc., Tokyo, Japan) to completely inactivate the virus.[7] This grid preparation was performed at the P3 facility of Hiroshima University under Biosafety Level 3 regulations. The sample grids were observed using TEM (JEOL, JEM-1400) with a tungsten filament operated at 80 kV at the Natural Science Center for Basic Research and Development, Hiroshima University. The images were recorded on a CCD camera (1024 × 1024 pixels).

References

1. Bruker, *APEX3, SADAB5, SAINT*, **2016**.
2. G. M. Sheldrick, *Acta Crystallogr., Sect. A Found. Crystallogr* **2008**, *64*, 112–122.
3. G. M. Sheldrick, *Acta Crystallogr., Sect. C Struct. Chem.* **2015**, *71*, 3–8.
4. C. B. Hübschle, G. M. Sheldrick, B. Dittrich, *J. Appl. Crystallogr.* **2011**, *44*, 1281–1284.
5. N. C. Sukmana, J. Shinogi, A. Yamamoto, A. Higashiura, T. Sakaguchi, M. Sadakane, *Eur. J. Inorg. Chem.* **2022**, e202200322.
6. T. Kawahara, I. Akiba, M. Sakou, T. Sakaguchi, H. Taniguchi, *PLoS One* **2018**, *13*, e0204908.
7. H. Kitagawa, T. Nomura, T. Nazmul, K. Omori, N. Shigemoto, T. Sakaguchi, H. Ohge, *Am. J. Infect. Control* **2021**, *49*, 299–301.

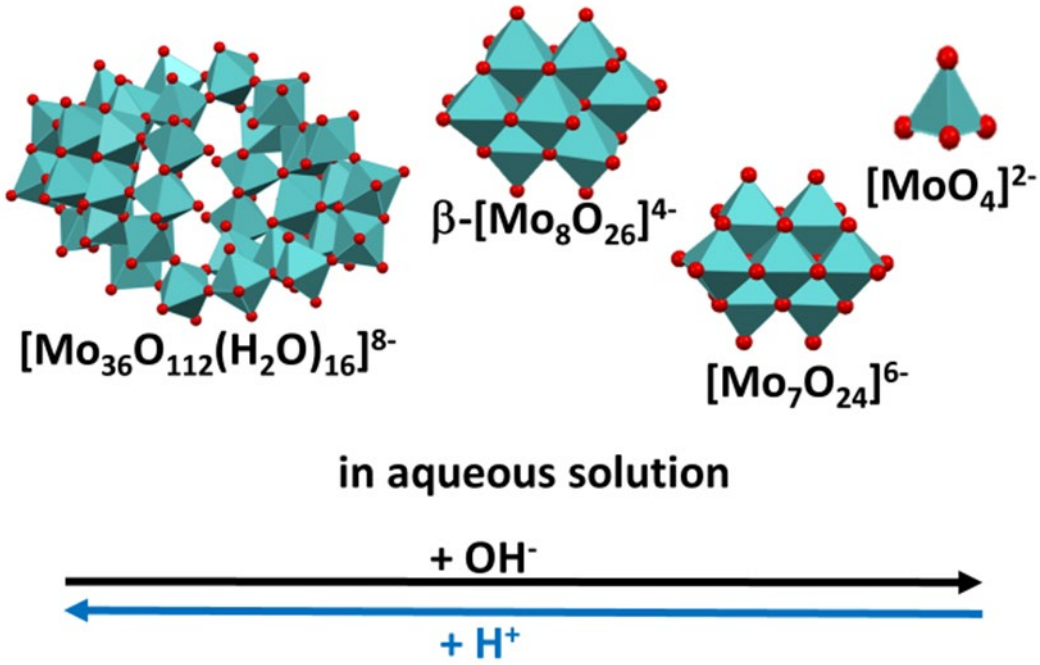

Scheme S1. Effect of acidity on the formation of isopolymolybdates in aqueous solutions.

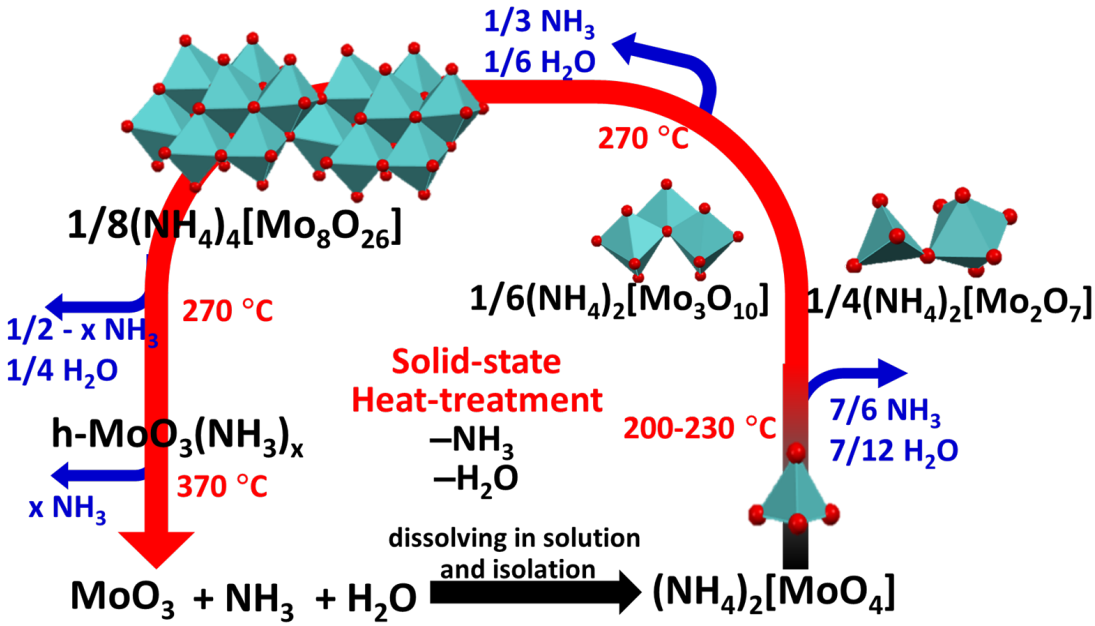

Scheme S2. Formation of ammonium monomolybdate via the reaction of MoO_3, H_2O, and NH_3, and its solid-state thermal transformation.

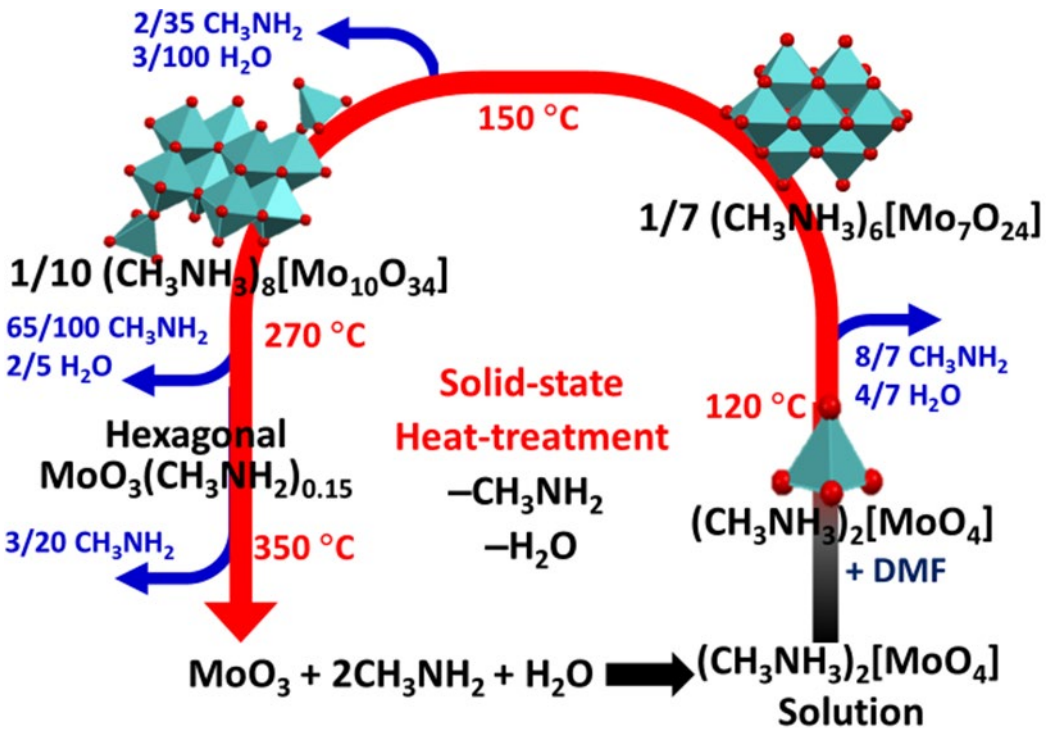

Scheme S3. Formation of methylammonium monomolybdate via the reaction of MoO_3, H_2O, and CH_3NH_2, and its solid-state thermal transformation.

Table S1. Crystal data for methylammonium isopolyoxomolybdates

Empirical Formula	$(CH_3NH_3)_2[MoO_4]$	$(CH_3NH_3)_6[Mo_7O_{24}]$	$(CH_3NH_3)_8[Mo_{10}O_{34}]\cdot 2H_2O$	$(CH_3NH_3)_8[Mo_{10}O_{34}]\cdot 2H_2O$
M.W. (g/mol)	224.08	1247.99	1795.9	1795.9
Temp. (K)	90	90	295	100
Crystal system	Orthorhombic	Triclinic	Monoclinic	Monoclinic
Space group	*Pnma*	$P\bar{1}$	$P2_1/n$	$P2_1/n$
a (Å)	9.3684(18)	10.4409(7)	12.596(2)	10.5245(8)
b (Å)	6.8961(13)	10.8297(8)	17.175(2)	17.1868(13)
c (Å)	11.911(2)	16.0303(11)	10.653(2)	12.5003(9)
α (°)	90	100.611(1)	90	90
β (°)	90	90.909(1)	91.04(2)	91.1630(10)
γ (°)	90	118.343(1)	90	90
V (Å^3)	769.5(3)	1556.79	2304.25	2260.6(3)
Z	4	2	2	2
$D_{calcd.}$ (g/cm^{-3})	1.934	2.662	2.588	2.683
μ (mm^{-1})	1.663	2.825		2,783
Radiation				
F(000)	448.0	1200.0		1728
Index ranges	$-8 \le h \le 12$ $-8 \le k \le 9$ $-15 \le l \le 14$	$-13 \le h \le 13$ $-14 \le k \le 14$ $-20 \le l \le 21$		$-13 \le h \le 13$ $-22 \le k \le 22$ $-16 \le l \le 16$
G.O.F.	1.048	1.045		1.017
R indexes [$I > 2\sigma(I)$]	$R_1 = 0.0206$; $wR_2 = 0.0480$	$R_1 = 0.0169$; $wR_2 = 0.0395$	$R_1 = 0.041$; $wR_2 = 0.041$	$R_1 = 0.0227$; $wR_2 = 0.0474$
R indexes [all data]	$R_1 = 0.0290$; $wR_2 = 0.0520$	$R_1 = 0.0192$; $wR_2 = 0.0403$		$R_1 = 0.0301$; $wR_2 = 0.0227$
	This study	*This study*	*reported by Yamase*[8]	*This study*

8. P. K. Bharadwaj, Y. Ohashi, Y. Sasada, Y. Sasaki, T. Yamase, *Acta Crystallogr., Sect. C Struct. Chem.* **1986**, *42*, 545–547.

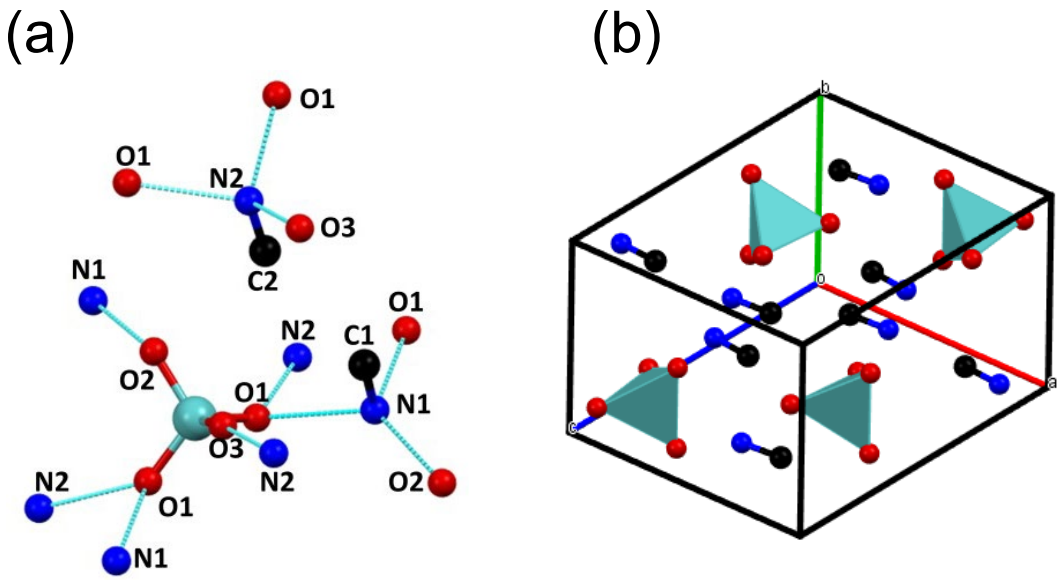

Figure S1. (a) Ball-and-stick representation and atom labeling for methylammonium monomolybdate, and (b) packing of molecules in a unit cell. Hydrogen atoms are not shown for clarity. Light blue, red, black, and blue balls represent molybdenum, oxygen, carbon, and nitrogen atoms, respectively. Light blue lines represent the hydrogen bonds between N and O atoms, which are shorter than 3.0 Å.

Table S2. Selected O–Mo–O angles (°) of $[MoO_4]^{2-}$.

Bonds	Angle (°)
O2-Mo1-O3	109.95(10)
O2-Mo1-O1	109.95(6)
O3-Mo1-O1	108.98(6)
O2-Mo1-O1	109.95(6)
O3-Mo1-O1	108.98(6)
O1-Mo1-O1	109.00(10)

Table S3. Selected bond distances (Å) of $[MoO_4]^{2-}$.

Bonds	Length (Å)
Mo1-O2	1.748(2)
Mo1-O3	1.755(2)
Mo1-O1	1.7800(15)
Mo1-O1	1.7801(15)

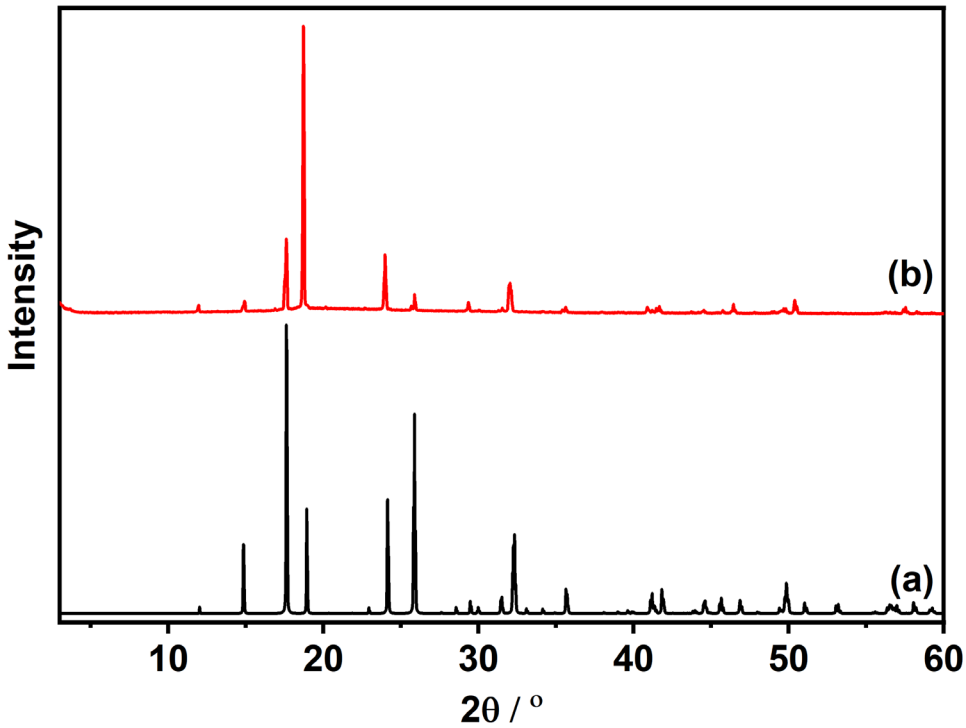

Figure S2. XRD patterns of methylammonium monomolybdate, $(CH_3NH_3)_2[MoO_4]$: (a) simulated pattern obtained from single crystal X-ray structure analysis data and (b) observed pattern.

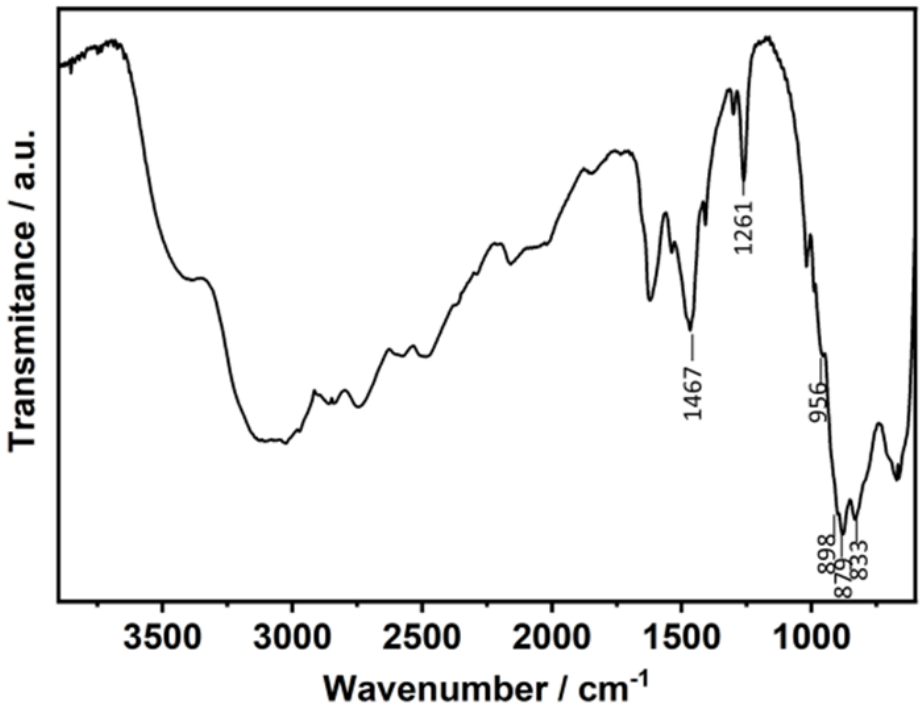

Figure S3. FT-IR spectrum of methylammonium monomolybdate, $(CH_3NH_3)_2[MoO_4]$.

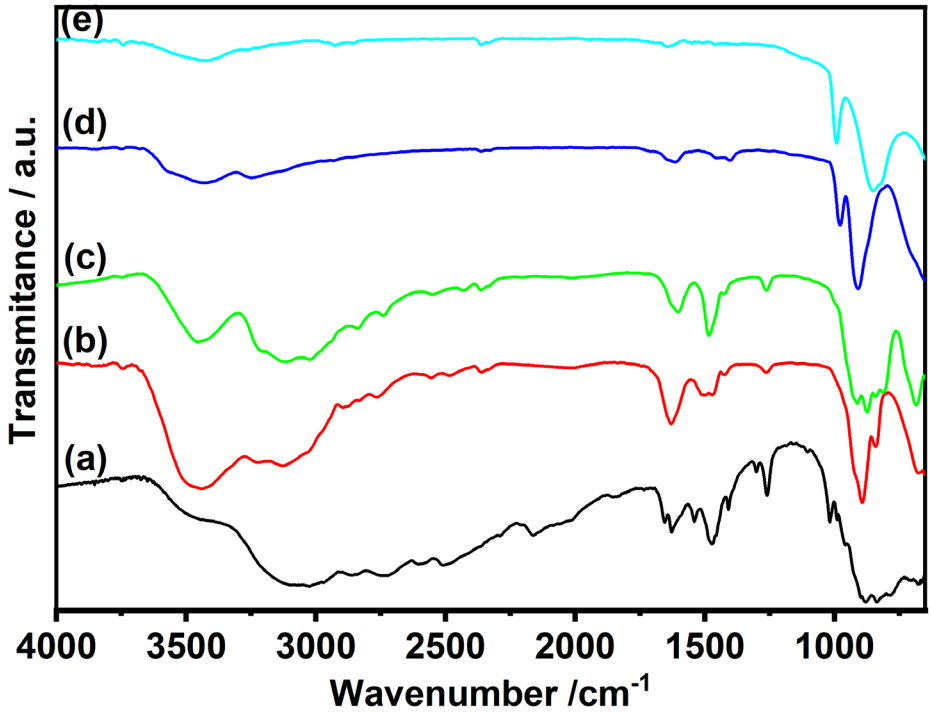

Figure S4. FT-IR spectra of (a) methylammonium monomolybdate calcined at (b) 120, (c) 150, (d) 270, and (e) 350 °C.

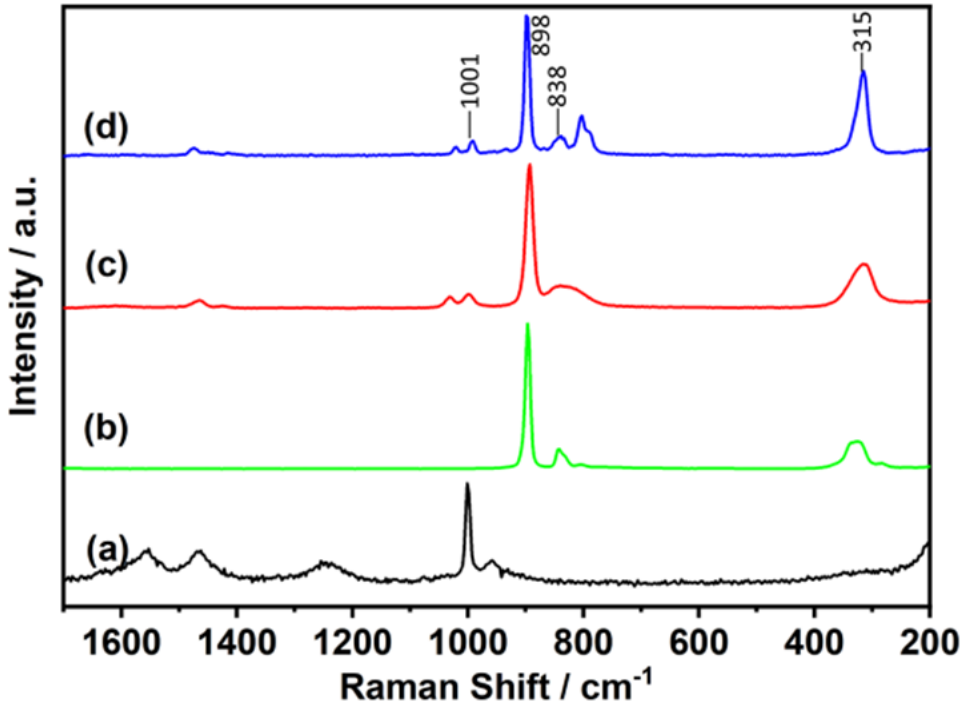

Figure S5. Raman spectra of (a) methylamine hydrochloride, $CH_3NH_3^+Cl^-$, (b) sodium monomolybdate, $Na_2[MoO_4]$, and (c) methylammonium monomolybdate, $(CH_3NH_3)_2[MoO_4]$ prepared in the synthesis solution, and (d) isolated $(CH_3NH_3)_2[MoO_4]$ solid.

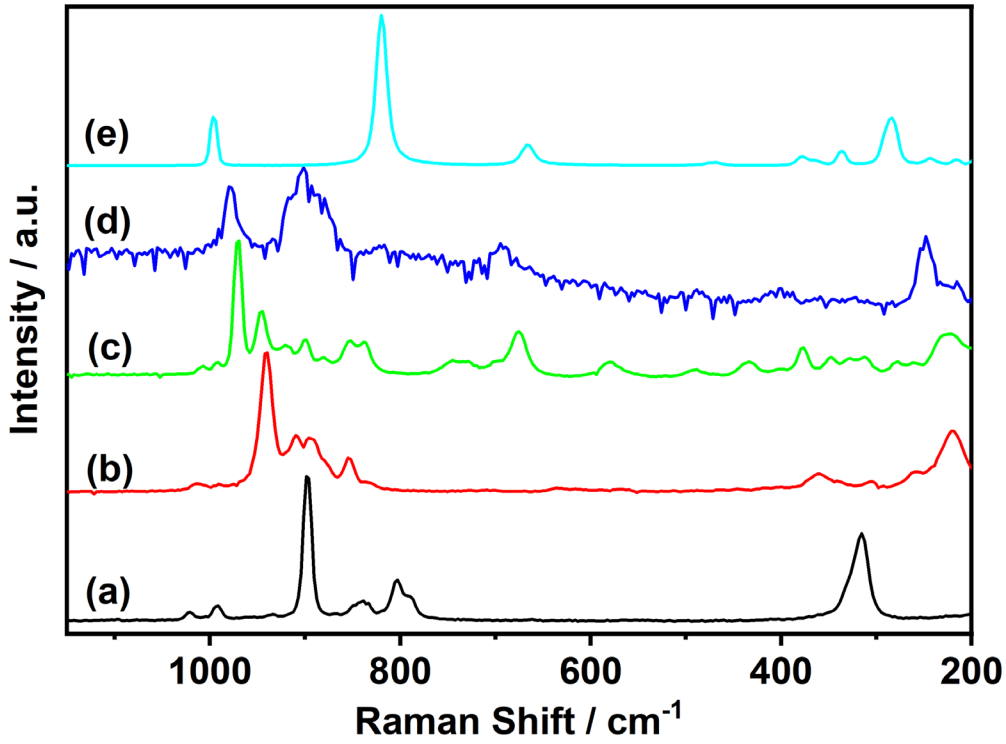

Figure S6. Raman spectra of (a) methylammonium monomolybdate calcined at (b) 120, (c) 150, (d) 270, and (e) 350 °C.

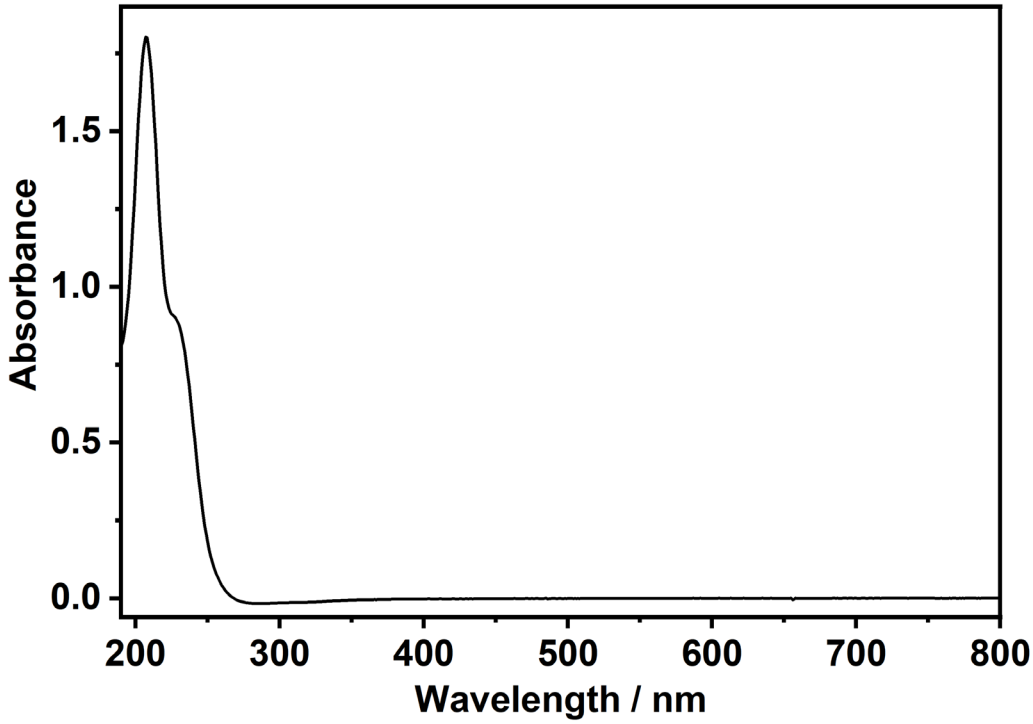

Figure S7. UV–vis spectrum of solution the reaction of MoO_3 and methylamine (solution concentration: 5 μL/50 mL H_2O).

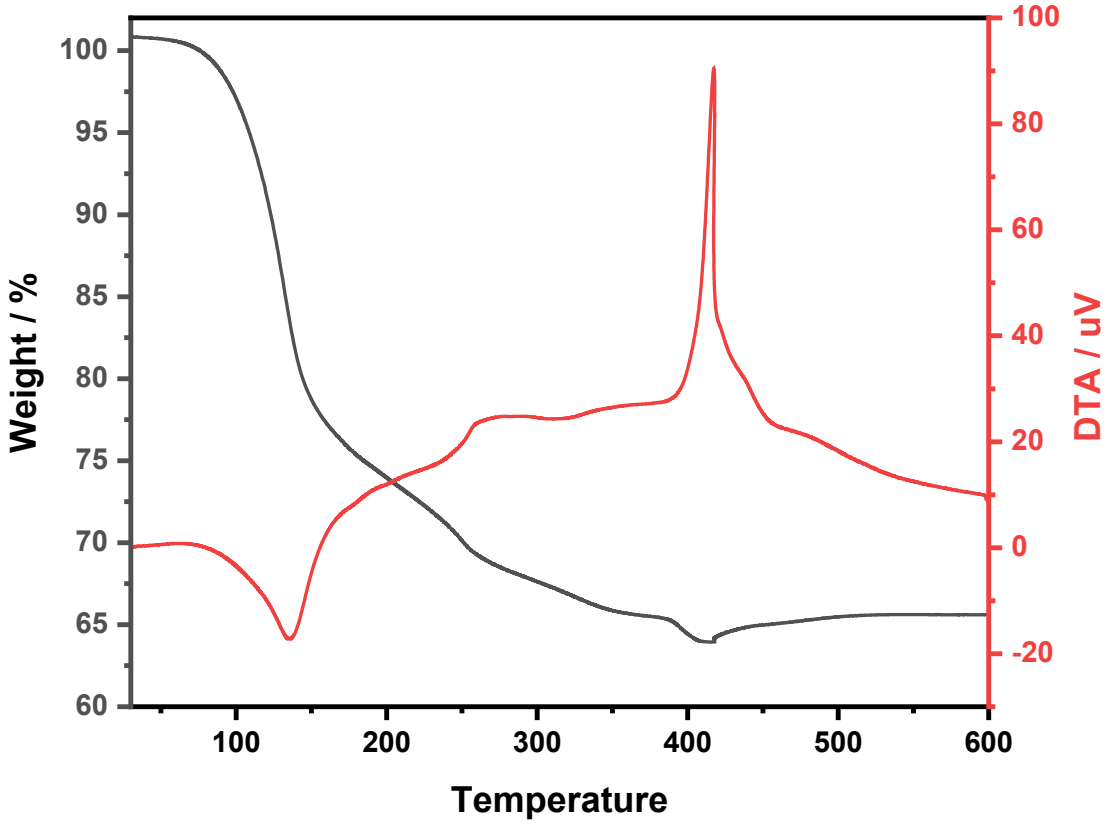

Figure S8. TG/DTA curves of methylammonium monomolybdate under air flow.

Table S4. Formula for methylammonium isopolymolybdate estimated by TG and CHN elemental analysis.

Formula	Weight Loss (wt%)[a] Calc.(obs.)	C (wt%) Calc.(obs.)	H (wt%) Calc.(obs.)	N (wt%) Calc.(obs.)
$(CH_3NH_3)_2[MoO_4]$	35.8(36.1)	9.92(10.09)	5.84(5.36)	11.57(11.60)
$(CH_3NH_3)_6[Mo_7O_{24}]$	19.3(19.1)	5.77(5.45)	2.91(2.77)	6.74(6.11)
$(CH_3NH_3)_8[Mo_{10}O_{34}]\cdot 2H_2O$	19.9(20.3)	5.35(5.15)	2.92(2.62)	6.24(5.85)
Hexagonal-$MoO_3(CH_3NH_2)_{0.15}$	2.9(2.4)	1.21(0.99)	0.51(0.28)	1.41(1.56)

[a] estimated by TG-DTA under air flow up to approximately 500 °C.

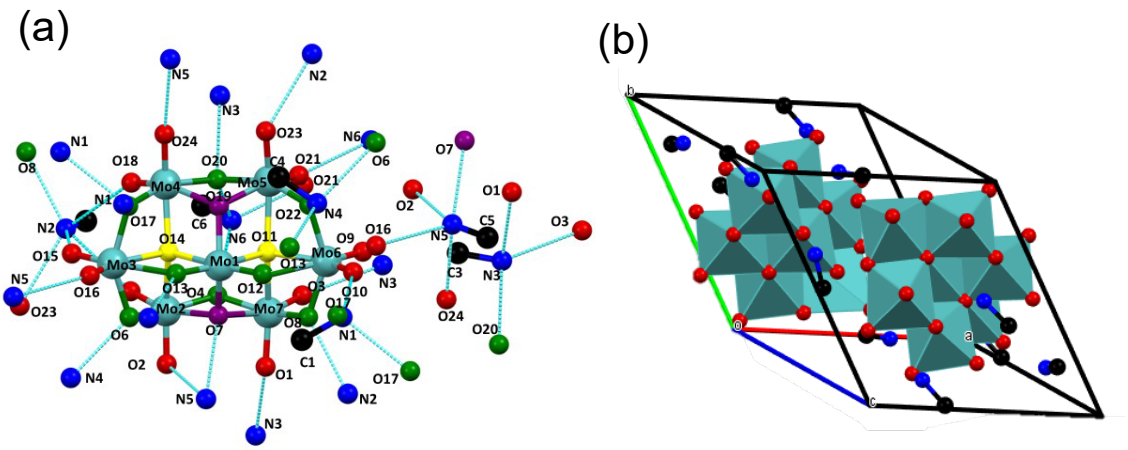

Figure S9. (a) Ball-and-stick representation and atom labeling for methylammonium heptamolybdate and (b) packing of molecules in a unit cell. Hydrogen atoms are not shown for clarity. Light blue, red, green, purple, yellow, black, and blue balls represent molybdenum, terminal oxygen, two-fold coordinated oxygen, three-fold coordinated oxygen, four-fold coordinated oxygen, carbon, and nitrogen atoms, respectively. Light blue lines represent the hydrogen bonds between N and O atoms, which are shorter than 3.0 Å.

Table S5. Selected bond distance (Å) for $[Mo_7O_{24}]^{6-}$

Bonds	Length (Å)	Bonds	Length (Å)
Mo1-O12	1.7282(15)	Mo4-O17	1.9995(15)
Mo1-O13	1.7563(15)	Mo4-O14	2.1557(14)
Mo1-O19	1.8993(14)	Mo4-O19	2.2865(15)
Mo1-O7	1.9090(15)	Mo5-O21	1.7163(16)
Mo1-O11	2.2516(14)	Mo5-O23	1.7216(15)
Mo1-O14	2.2723(14)	Mo5-O22	1.9060(15)
Mo2-O5	1.7112(15)	Mo5-O20	2.0094(15)
Mo2-O2	1.7122(15)	Mo5-O19	2.1625(15)
Mo2-O4	1.9410(15)	Mo5-O11	2.2734(14)
Mo2-O6	2.0009(15)	Mo6-O9	1.7125(16)
Mo2-O14	2.1687(14)	Mo6-O10	1.7248(15)
Mo2-O7	2.2925(15)	Mo6-O8	1.9199(15)
Mo3-O15	1.7108(15)	Mo6-O22	1.9454(15)
Mo3-O16	1.7451(15)	Mo6-O11	2.1272(14)
Mo3-O6	1.9015(15)	Mo6-O12	2.6390
Mo3-O17	1.9271(15)	Mo7-O3	1.7162(15)
Mo3-O14	2.1528(14)	Mo7-O1	1.7350(15)
Mo3-O13	2.4856(15)	Mo7-O4	1.9354(15)
Mo4-O18	1.7085(15)	Mo7-O8	1.9744(15)
Mo4-O24	1.7204(15)	Mo7-O11	2.1817(14)
Mo4-O20	1.9335(15)	Mo7-O7	2.2464(15)

Table S6. Selected O–Mo–O angles (°) of $[Mo_7O_{24}]^{6-}$

Bonds	Angle (°)	Bonds	Angle (°)	Bonds	Angle (°)
O12-Mo1-O13	104.76(7)	O12-Mo1-O13	104.76(7)	O12-Mo1-O13	104.76(7)
O12-Mo1-O19	101.27(7)	O16-Mo3-O13	78.98(6)	O9-Mo6-O11	104.66(6)
O13-Mo1-O19	100.02(7)	O6-Mo3-O13	81.07(6)	O10-Mo6-O11	148.04(7)
O12-Mo1-O7	102.27(7)	O17-Mo3-O13	79.00(6)	O8-Mo6-O11	75.58(6)
O13-Mo1-O7	101.14(7)	O14-Mo3-O13	70.11(5)	O22-Mo6-O11	75.39(6)
O19-Mo1-O7	142.95(6)	O18-Mo4-O24	105.19(7)	O3-Mo7-O1	106.12(8)
O12-Mo1-O11	84.95(6)	O18-Mo4-O20	97.70(7)	O3-Mo7-O4	96.28(7)
O13-Mo1-O11	170.28(6)	O24-Mo4-O20	98.18(7)	O1-Mo7-O4	100.76(7)
O19-Mo1-O11	77.29(6)	O18-Mo4-O17	101.42(7)	O3-Mo7-O8	99.58(7)
O7-Mo1-O11	76.75(6)	O24-Mo4-O17	91.67(7)	O1-Mo7-O8	92.06(7)
O12-Mo1-O14	172.97(6)	O20-Mo4-O17	155.37(6)	O4-Mo7-O8	155.97(6)
O13-Mo1-O14	82.25(6)	O18-Mo4-O14	91.80(7)	O3-Mo7-O11	94.16(6)
O19-Mo1-O14	76.60(6)	O24-Mo4-O14	159.16(7)	O1-Mo7-O11	156.83(7)
O7-Mo1-O14	76.54(6)	O20-Mo4-O14	91.24(6)	O4-Mo7-O11	87.75(6)
O11-Mo1-O14	88.04(5)	O17-Mo4-O14	72.88(6)	O8-Mo7-O11	73.26(6)
O5-Mo2-O2	106.26(8)	O18-Mo4-O19	160.11(6)	O3-Mo7-O7	163.44(7)
O5-Mo2-O4	98.68(7)	O24-Mo4-O19	93.48(6)	O1-Mo7-O7	89.49(6)
O2-Mo2-O4	99.72(7)	O20-Mo4-O19	72.42(6)	O4-Mo7-O7	74.96(6)
O5-Mo2-O6	101.36(7)	O17-Mo4-O19	84.55(6)	O8-Mo7-O7	85.01(6)
O2-Mo2-O6	90.73(7)	O14-Mo4-O19	71.64(5)	O11-Mo7-O7	71.79(5)
O4-Mo2-O6	153.79(6)	O21-Mo5-O23	105.01(8)	Mo6-O11-Mo7	94.39(6)
O5-Mo2-O14	93.16(7)	O21-Mo5-O22	101.17(7)	Mo6-O11-Mo1	104.07(6)
O2-Mo2-O14	156.72(7)	O23-Mo5-O22	99.21(7)	Mo7-O11-Mo1	100.72(6)
O4-Mo2-O14	89.67(6)	O21-Mo5-O20	89.19(7)	Mo6-O11-Mo5	93.37(5)
O6-Mo2-O14	72.58(6)	O23-Mo5-O20	98.32(7)	Mo7-O11-Mo5	158.49(7)
O5-Mo2-O7	162.54(6)	O22-Mo5-O20	156.52(6)	Mo1-O11-Mo5	96.80(5)
O2-Mo2-O7	90.70(6)	O21-Mo5-O19	156.27(7)	Mo1-O13-Mo3	106.30(7)
O4-Mo2-O7	73.77(6)	O23-Mo5-O19	93.97(7)	Mo3-O14-Mo4	96.54(6)
O6-Mo2-O7	82.19(6)	O22-Mo5-O19	89.46(6)	Mo3-O14-Mo2	95.48(6)
O14-Mo2-O7	71.41(5)	O20-Mo5-O19	73.84(6)	Mo4-O14-Mo2	150.94(7)
O15-Mo3-O16	105.82(7)	O21-Mo5-O11	90.89(7)	Mo3-O14-Mo1	101.29(6)
O15-Mo3-O6	99.57(7)	O23-Mo5-O11	163.44(7)	Mo4-O14-Mo2	101.57(6)
O16-Mo3-O6	102.55(7)	O22-Mo5-O11	72.69(6)	Mo2-O14-Mo2	101.87(6)
O15-Mo3-O17	98.12(7)	O20-Mo5-O11	86.28(6)	Mo3-O17-Mo4	109.93(7)
O16-Mo3-O17	98.54(7)	O19-Mo5-O11	71.93(5)	Mo1-O19-Mo5	112.67(7)
O6-Mo3-O17	147.49(6)	O9-Mo6-O10	107.22(7)	Mo1-O19-Mo4	109.78(7)
O15-Mo3-O14	105.02(7)	O9-Mo6-O8	100.77(7)	Mo5-O19-Mo4	95.95(6)
O16-Mo3-O14	149.04(7)	O10-Mo6-O8	100.44(7)	Mo4-O20-Mo5	113.94(7)
O6-Mo3-O14	74.84(6)	O9-Mo6-O22	102.17(7)	Mo5-O22-Mo6	112.56(7)
O17-Mo3-O14	74.33(6)	O10-Mo6-O22	95.53(7)		

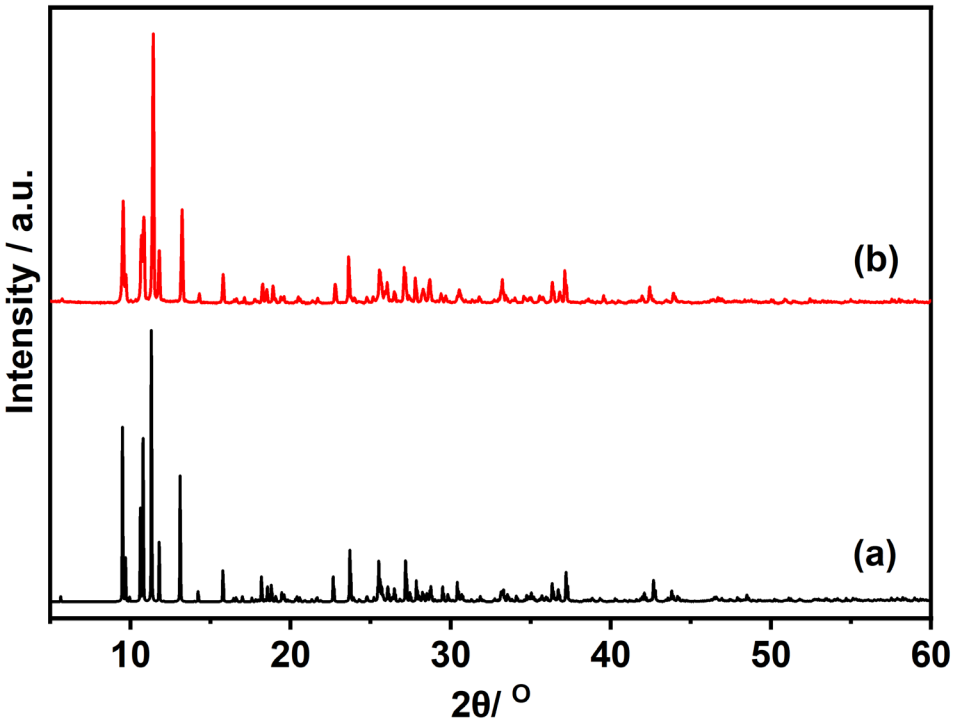

Figure S10. XRD patterns of methylammonium heptamolybdate, $(CH_3NH_3)_6[Mo_7O_{24}]$: (a) simulated pattern obtained from single-crystal X-ray structure analysis data and (b) observed pattern.

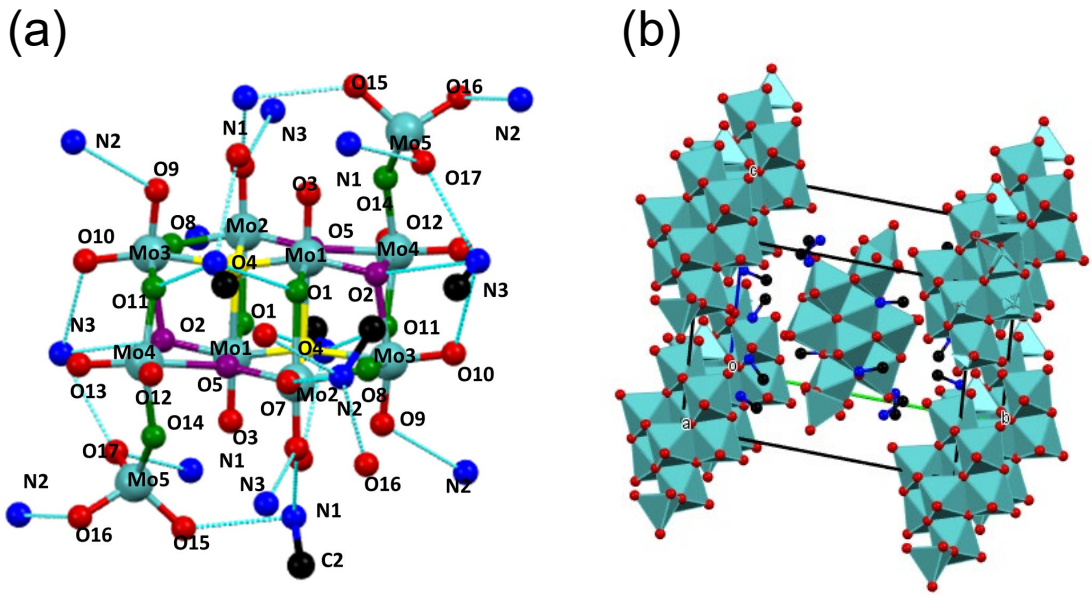

Figure S11. (a) Ball-and-stick representation and atom labeling for methylammonium decamolybdate and (b) packing of molecules in a unit cell. Hydrogen atoms are not shown for clarity. Light blue, red, green, purple, yellow, black, and blue balls represent molybdenum, terminal oxygen, two-fold coordinated oxygen, three-fold coordinated oxygen, four-fold coordinated oxygen, carbon, and nitrogen atoms, respectively. Light blue lines represent the hydrogen bonds between N and O atoms, which are shorter than 3.0 Å.

Table S7. Selected bond distances (Å) of $[Mo_{10}O_{34}]^{8-}$

Bonds	Length (Å)	Bonds	Length (Å)
Mo1-O3	1.699(2)	Mo3-O11	1.929(2)
Mo1-O1	1.765(2)	Mo3-O8	1.949(2)
Mo1-O2	1.864(2)	Mo3-O4	2.224(2)
Mo1-O4	1.955(2)	Mo3-O2	2.281(2)
Mo1-O5	2.137(2)	Mo4-O12	1.702(2)
Mo1-O4	2.426(2)	Mo4-O13	1.713(2)
Mo2-O7	1.721(2)	Mo4-O11	1.916(2)
Mo2-O6	1.724(2)	Mo4-O14	2.022(2)
Mo2-O8	1.903(2)	Mo4-O5	2.163(2)
Mo2-O5	1.908(2)	Mo4-O2	2.270(2)
Mo2-O4	2.230(2)	Mo5-O16	1.745(2)
Mo2-O1	2.340(2)	Mo5-O15	1.747(2)
Mo3-O10	1.714(2)	Mo5-O17	1.756(2)
Mo3-O9	1.723(2)	Mo5-O14	1.813(2)

Table S8. Selected O–Mo–O angles (°) of $[Mo_{10}O_{34}]^{8-}$

Bonds	Angle (°)	Bonds	Angle (°)	Bonds	Angle (°)
O3-Mo1-O1	104.30(10)	O6-Mo2-O4	100.11(9)	O4-Mo3-O2	73.61(7)
O3-Mo1-O2	103.93(9)	O8-Mo2-O4	73.52(8)	O12-Mo4-O13	105.95(10)
O1-Mo1-O2	100.65(9)	O5-Mo2-O4	72.00(8)	O12-Mo4-O11	99.03(10)
O3-Mo1-O4	102.52(9)	O7-Mo2-O1	85.33(9)	O13-Mo4-O11	99.34(10)
O1-Mo1-O4	97.48(9)	O6-Mo2-O1	171.63(9)	O12-Mo4-O14	97.99(10)
O2-Mo1-O4	142.90(9)	O8-Mo2-O1	79.28(8)	O13-Mo4-O14	90.99(10)
O3-Mo1-O5	98.33(9)	O5-Mo2-O1	79.88(8)	O11-Mo4-O14	156.79(8)
O1-Mo1-O5	156.99(9)	O4-Mo2-O1	71.62(7)	O12-Mo4-O5	93.71(9)
O2-Mo1-O5	77.55(8)	O10-Mo3-O9	105.33(10)	O13-Mo4-O5	158.63(9)
O4-Mo1-O5	73.26(8)	O10-Mo3-O11	99.98(9)	O11-Mo4-O5	85.46(8)
O3-Mo1-O4	177.80(8)	O9-Mo3-O11	97.13(9)	O14-Mo4-O5	77.80(8)
O1-Mo1-O4	77.55(8)	O10-Mo3-O8	94.96(9)	O12-Mo4-O2	161.81(9)
O2-Mo1-O4	76.74(8)	O9-Mo3-O8	101.19(9)	O13-Mo4-O2	91.99(9)
O4-Mo1-O4	75.97(8)	O11-Mo3-O8	152.35(9)	O11-Mo4-O2	74.58(8)
O5-Mo1-O4	79.74(7)	O10-Mo3-O4	159.87(9)	O14-Mo4-O2	84.40(8)
O7-Mo2-O6	102.97(10)	O9-Mo3-O4	92.94(9)	O5-Mo4-O2	69.07(7)
O7-Mo2-O8	104.24(9)	O11-Mo3-O4	85.79(8)	O16-Mo5-O15	107.54(10)
O6-Mo2-O8	97.38(9)	O8-Mo3-O4	72.83(8)	O16-Mo5-O17	106.91(10)
O7-Mo2-O5	103.13(9)	O10-Mo3-O2	89.32(9)	O15-Mo5-O17	110.13(10)
O6-Mo2-O5	99.02(9)	O9-Mo3-O2	164.21(9)	O16-Mo5-O14	108.22(10)
O8-Mo2-O5	143.84(9)	O11-Mo3-O2	74.10(8)	O15-Mo5-O14	111.09(10)
O7-Mo2-O4	156.90(9)	O8-Mo3-O2	83.01(8)	O17-Mo5-O14	112.71(10)

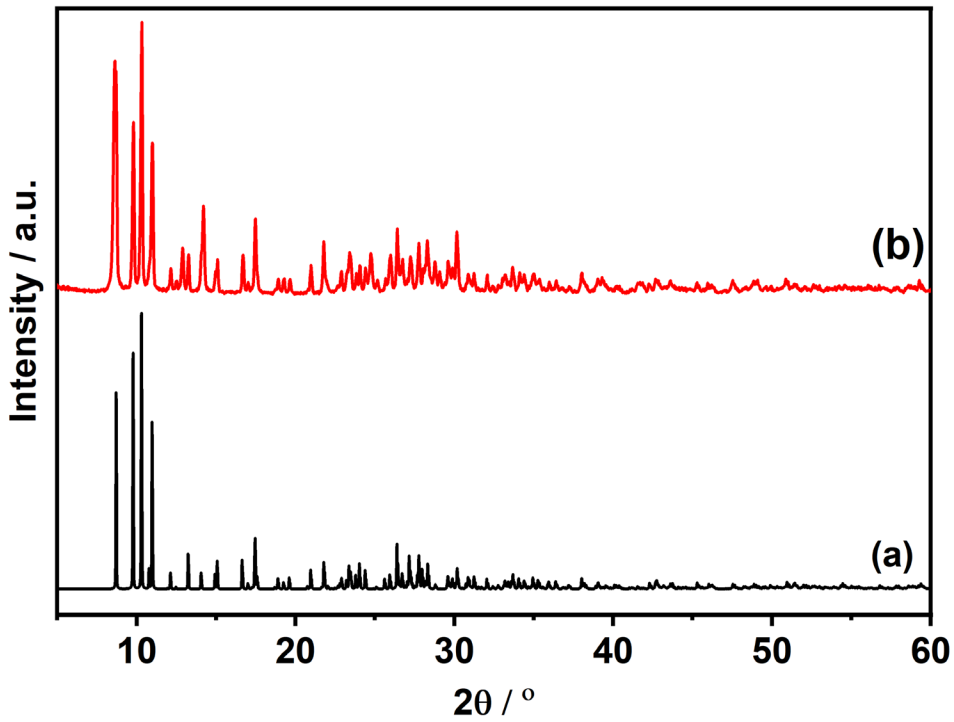

Figure S12. XRD patterns of methylammonium decamolybdate, $(CH_3NH_3)_8[Mo_{10}O_{34}]\cdot 2H_2O$, (a) simulated pattern obtained from single-crystal X-ray structure analysis data and (b) observed pattern.

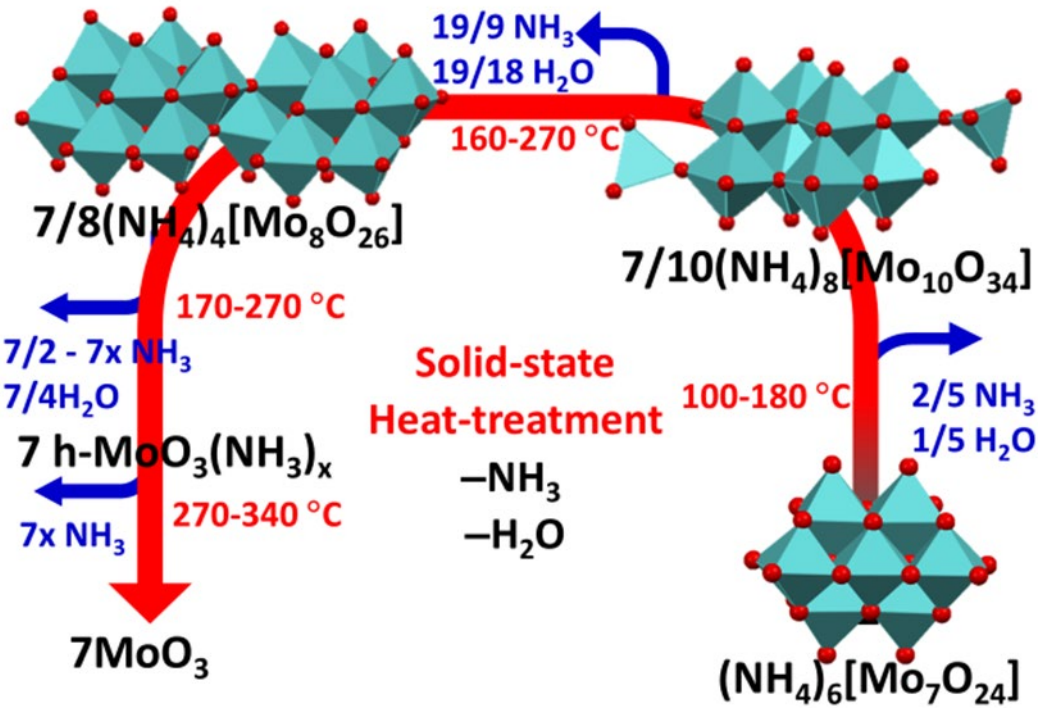

Scheme S4. Solid-state thermal transformation of ammonium heptamolybdate.

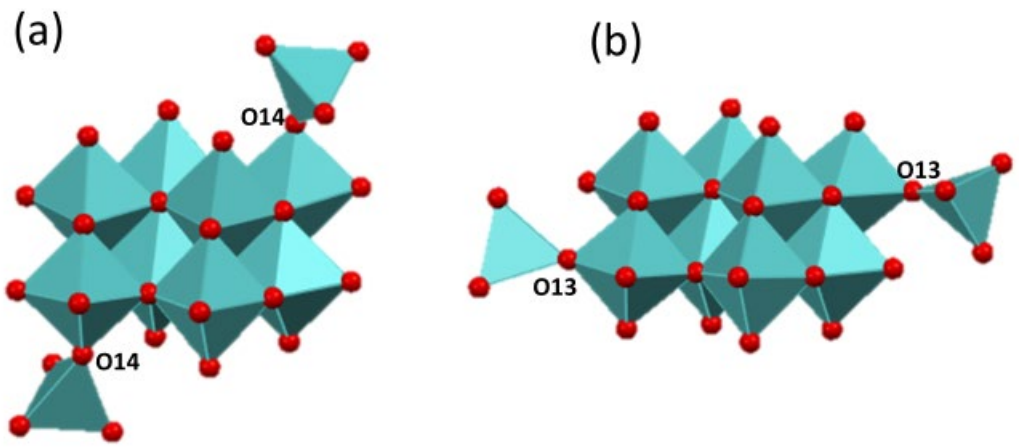

Figure S13. Polyhedral representation of the $[Mo_{10}O_{34}]^{8-}$ anions of (a) methylammonium decamolybdate and (b) ammonium decamolybdate (ICSD 67325).

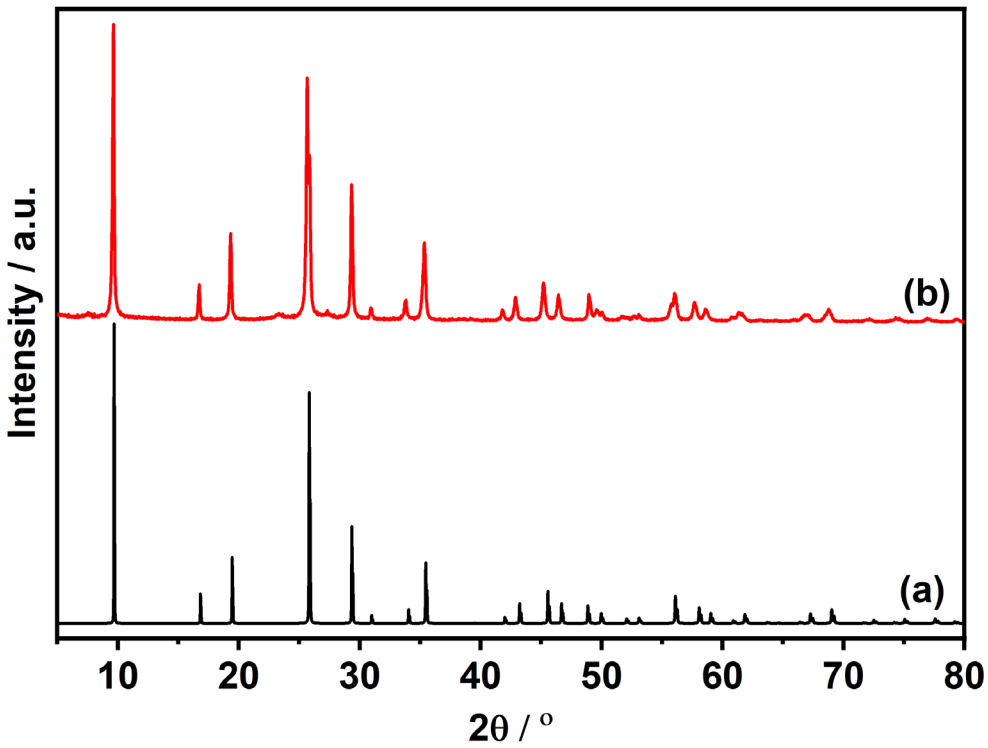

Figure S14. XRD patterns of hexagonal MoO_3: (a) simulated pattern obtained from structural data provided in ICDD 21-0569 and (b) observed pattern of the obtained solid heating at 270 °C for 1 hour.

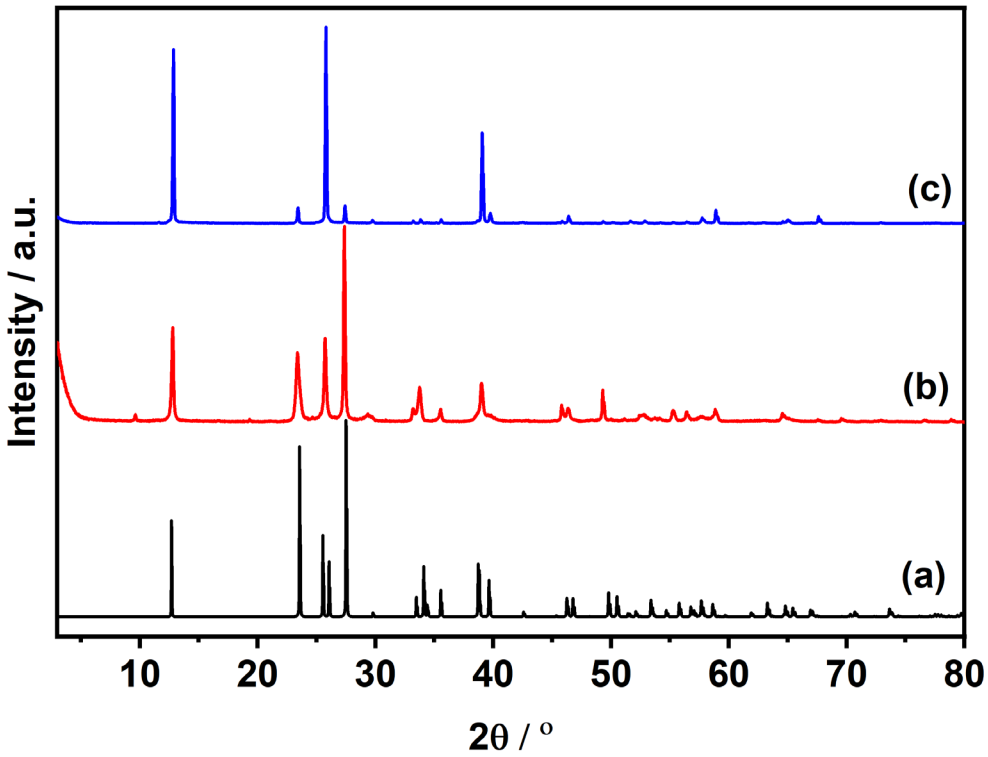

Figure S15. XRD patterns of orthorhombic MoO_3: (a) simulated pattern obtained from structural data provided in ICDD 12-8070, (b) observed pattern of the obtained solid heating at 350 °C for 1 hour, and (c) observed pattern of the obtained solid heating at 500 °C for 1 hour.